

Synthesis and properties of $\text{BaCe}_{1-x}\text{Y}_x\text{O}_{3-\delta}$ – BaWO_4 composite protonic conductors

Agnieszka Łącz · Paweł Pasierb

Received: 15 November 2012 / Accepted: 18 February 2013 / Published online: 19 March 2013
© The Author(s) 2013. This article is published with open access at Springerlink.com

Abstract Barium cerate doped by trivalent rare earth metal ions is a potentially huge component of materials for electrochemical industry due to its high protonic conductivity. However, the poor chemical stability especially in the presence of CO_2 , SO_2 or H_2O , resulting in decreasing the mechanical durability of obtained materials, limits their possible applications. The new approach towards stable ceramic protonic conductors with high electrical conductivity is presented. Thermal stability of yttrium doped (10 mol%) of BaCeO_3 was enhanced by forming the composite material $\text{BaCe}_{0.9}\text{Y}_{0.1}\text{O}_3$ – BaWO_4 (10 mol% of BaWO_4). The synthesis was performed by solid-state reaction method. The detailed study of thermal decomposition of starting powders mixture was performed using thermogravimetry and differential thermal analysis (TG/DTA) techniques combined with Evolved Gas Analysis (EGA—mass spectrometry). Structure, phase composition and microstructure together with thermal stability of sintered materials were determined. The exposition tests were performed to characterise the stability of composites in carbon dioxide and water vapour-rich atmospheres. The samples were exposed to atmosphere containing $\text{CO}_2/\text{H}_2\text{O}$ (7 % of CO_2 in air, 100 % RH) at temperature of 25 °C for 300 h. Thermal analysis supplied with mass spectrometry was applied to analyse the materials after the test. The results of this experiment showed better chemical resistance of composite material— $\text{BaCe}_{0.9}\text{Y}_{0.1}\text{O}_3$ with 10 mol% of BaWO_4 compared to single phase material.

Keywords Protonic conductors · Barium cerate · Barium tungstate · Chemical stability · Perovskite type composite

Introduction

The development of solid oxide fuel cells, hydrogen pumps, gas separation membranes or gas sensors requires the materials where high protonic conductivity finds its applications [1–5]. Discovered by Iwahara et al. [6, 7], high protonic conductivity in perovskite type structure of barium and strontium cerates stimulated the development in the area of solid state electrochemistry. Modification of mechanical, chemical and electrical properties of ABO_3 perovskites by introducing acceptor dopants in the B-site, especially rare earth metal, was widely discussed and presented in the literature [8–15]. Many studies have been focused on the electrical conductivity of BaCeO_3 -based ceramics. Unfortunately, the chemical stability of proposed materials is still not satisfying. The secondary reactions of perovskite material used for construction of electrochemical devices with CO_2 and H_2O vapour, lead to the decomposition or even disintegration of the material due to deterioration of mechanical properties.

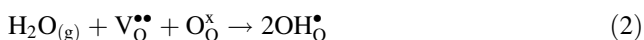
Introduction of acceptor dopant M^{3+} (like— Y^{3+} , Yb^{3+} , Nd^{3+} , Gd^{3+} , Ta^{3+}) at the amount up to 10 mol% to the perovskite type BaCeO_3 does not affect the crystallographic structure greatly [16] but leads to the increase of the concentration of oxygen vacancies (Kröger–Vink notation was used):



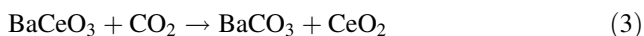
In water/hydrogen rich atmospheres, oxygen vacancies created according to Eq. (1) play a crucial role in the

A. Łącz (✉) · P. Pasierb
AGH University of Science and Technology,
Faculty of Materials Science and Ceramics,
30 Mickiewicz Av., 30-059 Kraków, Poland
e-mail: alacz@agh.edu.pl

formation of protonic defects which determine the value of protonic conductivity:



As mentioned previously, one of the greatest disadvantages of materials based on barium cerate is poor chemical stability especially in the presence of water and carbon dioxide where barium carbonate and cerium(IV) oxide are produced in the secondary reaction [17, 18]:



Based on thermodynamic data, the chemical stability of typical barium perovskites can be considered as follows: $\text{BaTiO}_3 > \text{BaZrO}_3 > \text{BaCeO}_3$ [17, 19]. Incorporation of zirconium into the doped barium cerate results in improving the chemical and mechanical stability [20, 21] but leads to decreasing of conductivity especially due to poor sinterability of barium zirconate. Similar results were obtained by doping BaCeO_3 with yttrium and titanium [22, 23].

The purpose of this study was to improve the chemical stability of single phase $\text{BaCe}_{1-x}\text{Y}_x\text{O}_3$ materials by introducing the second phase leading to synthesis of composite ceramic protonic conductors. As the second phase, the BaWO_4 was chosen. Barium tungstate, material commonly used in electrochemical, optical or gas sensor applications [24–26], is often prepared by solid state reaction method [27]. It is also known that introducing tungsten to perovskite type structure of $\text{Ba}(\text{Mg}_{1/3}\text{Ta}_{2/3})\text{O}_3$ results in formation of oxygen vacancies [28] which leads to the increase of protonic conductivity.

Experimental

Materials were prepared by solid-state reaction method. Barium carbonate, cerium(IV) oxide, water solution of yttrium(III) nitrate (0.28 M) and ammonium paratungstate hydrate were used as starting materials. All reagents were of analytical grade and were supplied by Aldrich Chemical Company. Samples with nominal compositions BaCeO_3 , $\text{BaCe}_{0.9}\text{Y}_{0.1}\text{O}_3$ and $0.9\text{BaCe}_{0.9}\text{Y}_{0.1}\text{O}_3-0.1\text{BaWO}_4$ were chosen for tests.

Appropriate amounts of starting powders were mixed, impregnated with required amount of water solution of $\text{Y}(\text{NO}_3)_3$ and dried at 80 °C for 12 h. Obtained powders were formed in the pellet die ($\phi = 10$ mm, pressure 2.0 MPa) and then calcined at 1,200 °C for 12 h. Calcination conditions were determined from TG/DTA results (SDT 2960 TA Instruments, mass about 50 mg, heating rate 10 °C min^{-1} , synthetic air atmosphere, platinum crucibles) as shown in the further part of this study. Obtained materials were crushed in agate mortar and again formed in the pellet

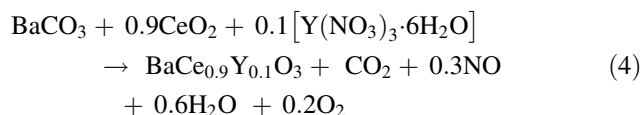
die ($\phi = 10$ mm, pressure 2.0 MPa), isostatically pressed (250 MPa) and sintered at 1,600 °C for 3 h in air atmosphere. Such sintered bodies were stored in a dessicator to avoid any secondary reactions.

X-ray diffraction XRD (Philips X'Pert with Cu K α radiation) and scanning electron microscopy SEM (Nova Nano SEM 200, FEI & Oxford Instruments) coupled with Electron Dispersive Spectrometry (EDS) (FEI & Oxford Instruments) techniques were used to determine microstructure, chemical and phase composition of obtained materials. Mass spectrometer (QMD 300 ThermoStar, Balzers) connected on-line with SDT 2960 apparatus by the quartz capillary heated up to 200 °C was applied to support the interpretation of TG/DTA results especially the stability of analysed materials in the presence of carbon dioxide.

Results and discussion

Sample preparation

The optimal preparation conditions were chosen based on the results of DTA/TG and XRD measurements. The general reaction of formation of yttrium doped barium cerate can be written as:



The mechanism of thermal decomposition of pure $\text{Y}(\text{NO}_3)_3 \cdot 6\text{H}_2\text{O}$ was precisely discussed in [29]. The complex composition of starting mixture and the material preparation leading to different decomposition pathways can be the reason for differences in the gaseous products reported in [29] and shown in the Eq. (4). It must be emphasised that the Eq. (4) describes only the stoichiometry, but not the mechanism of the reaction.

For composite material, the theoretical reaction of second phase formation can be proposed:

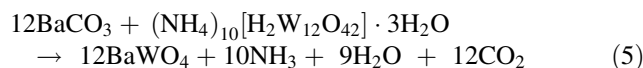


Figure 1 shows example of DTA-TG curves and MS results of starting mixture of powders. The analysis of mass spectrum of the gas produced by the powders decomposition shows the presence of carbon dioxide and nitrogen oxides. In the case of composite material also, ammonium was observed. As shown in Fig. 1, CO_2 is represented by the ion current curve for $m/z = 44$ (where M is mass of the molecule and z is a charge of the molecule in electron charge units); as in the mass spectrum for carbon dioxide, m/z equal to 44 is the most intense line. For the same reason, NH_3 is

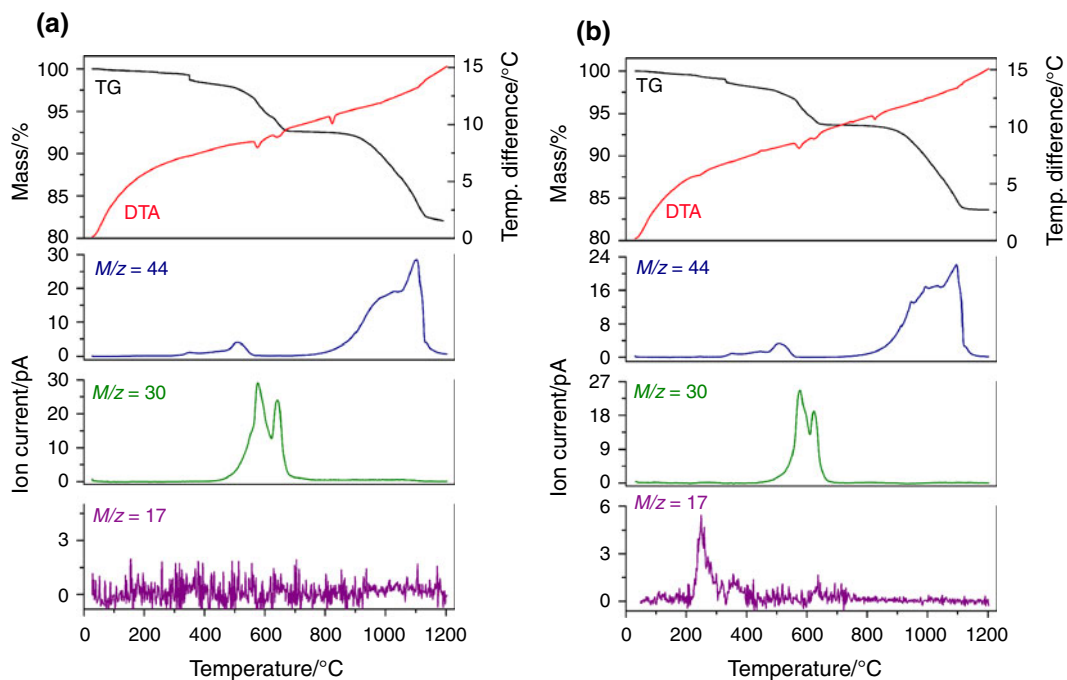


Fig. 1 TG/DTA/MS results for thermal decomposition of $\text{BaCe}_{0.9}\text{Y}_{0.1}\text{O}_3$ (a) and $0.9\text{BaCe}_{0.9}\text{Y}_{0.1}\text{O}_3\text{-}0.1\text{BaWO}_4$ (b) starting mixtures (nominal composition)

represented by the line for $m/z = 17$ and NO by the line m/z equal to 30. As can be seen for decomposition of $\text{BaCe}_{0.9}\text{Y}_{0.1}\text{O}_3$ starting mixture (Fig. 1a) below 400°C , only slight mass loss about 1.0 % is observed. It is probably caused by dehydration of the sample and/or desorption of H_2O and CO_2 . The mass loss in the temperature range $400\text{--}700^\circ\text{C}$ is caused by the emission of nitrogen oxides ($m/z = 30$) as a result of yttrium nitrate decomposition. Barium carbonate decomposes in the temperature range $800\text{--}1,200^\circ\text{C}$, which is illustrated in Fig. 1a by the mass loss observed on TG curve, very broad endothermic peak on DTA curve and releasing carbon dioxide—ion current $m/z = 44$. The results of $0.9\text{BaCe}_{0.9}\text{Y}_{0.1}\text{O}_3\text{-}0.1\text{BaWO}_4$ starting mixture decomposition are presented in Fig. 1b. The only difference in mass spectrometry analysis between these two starting mixtures is the presence of small amount of NH_3 in the gaseous product of the reaction. The ammonia is one of the major products of thermal decomposition of ammonium paratungstate hydrate $(\text{NH}_4)_{10}[\text{H}_2\text{W}_{12}\text{O}_{42}] \cdot 3\text{H}_2\text{O}$ which, according to the literature [30], decomposes in multistage process in the temperature range $90\text{--}450^\circ\text{C}$ leading to WO_3 as the final solid residue. The decomposition of ammonium paratungstate is not clearly seen on TG curve as the amount of this reagent in the starting mixture was only about 3 % and the temperature range of decomposition of these compounds is wide. Based on the results shown in Fig. 1, the optimal calcination temperature ($1,200^\circ\text{C}$) was proposed. The detailed procedure of calcination and sintering of the materials was presented in the Experimental part.

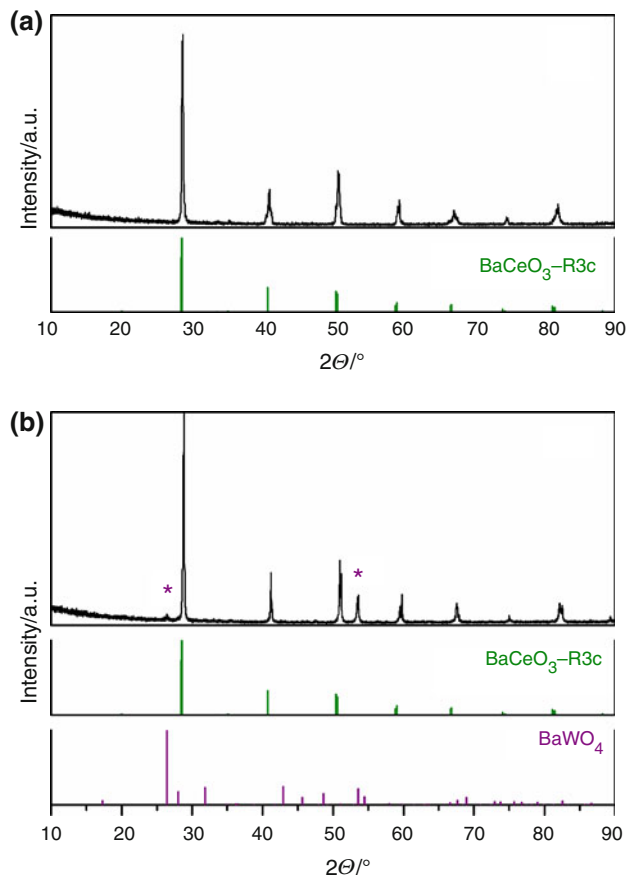


Fig. 2 XRD results of samples with nominal composition $\text{BaCe}_{0.9}\text{Y}_{0.1}\text{O}_3$ (a) and $0.9\text{BaCe}_{0.9}\text{Y}_{0.1}\text{O}_3\text{-}0.1\text{BaWO}_4$ (b)

Structure, phase composition and microstructure

Based on the XRD results, the phase composition and crystallographic structure were determined. Figure 2 shows the comparison of XRD data for different samples. It was found that in the case of $\text{BaCe}_{0.9}\text{Y}_{0.1}\text{O}_3$ sample, single phase perovskite material was found, interpreted as rhombohedral (space group $R-3c$, ICSD collection code: 088593). The calculated lattice constants were found to be $a = 0.62101$ nm, $c = 1.51514$ nm. In the case of sample with nominal composition $0.9\text{BaCe}_{0.9}\text{Y}_{0.1}\text{O}_3-0.1\text{BaWO}_4$, two phase material was detected. The BaCeO_3 perovskite rhombohedral was found as primary phase (space group $R-3c$, ICSD collection code: 088593), while tetragonal BaWO_4 (space group $I41/a$, ICSD collection code: 023702) was detected as a secondary phase, which is in general agreement with proposed phase composition. The calculated lattice

constants for BaCeO_3 were found to be $a = 0.62079$ nm, $c = 1.51212$ nm. As can be noticed, the change of lattice parameters was detected compared to single phase material. It suggests the modification of the crystallographic structure. Namely, the doping of W^{6+} into Ce^{4+} position is the most probable explanation, taking into account smaller ionic radii of W^{6+} ion ($r_{\text{W}} = 0.06$ nm for CN = 6) compared to the Ce^{4+} ion ($r_{\text{Ce}} = 0.087$ nm for CN = 6). The large difference between the ionic radii of both ions led to limited solubility of tungsten in barium cerate lattice and formation of BaWO_4 as the second phase, as assumed.

The BaWO_4 addition influences not only the phase composition and crystallographic structure but also the microstructure. Figure 3 shows the comparison of SEM images of $\text{BaCe}_{0.9}\text{Y}_{0.1}\text{O}_3$ and composite $0.9\text{BaCe}_{0.9}\text{Y}_{0.1}\text{O}_3-0.1\text{BaWO}_4$ samples. As can be seen, the difference between the grain size and the grain morphology of both

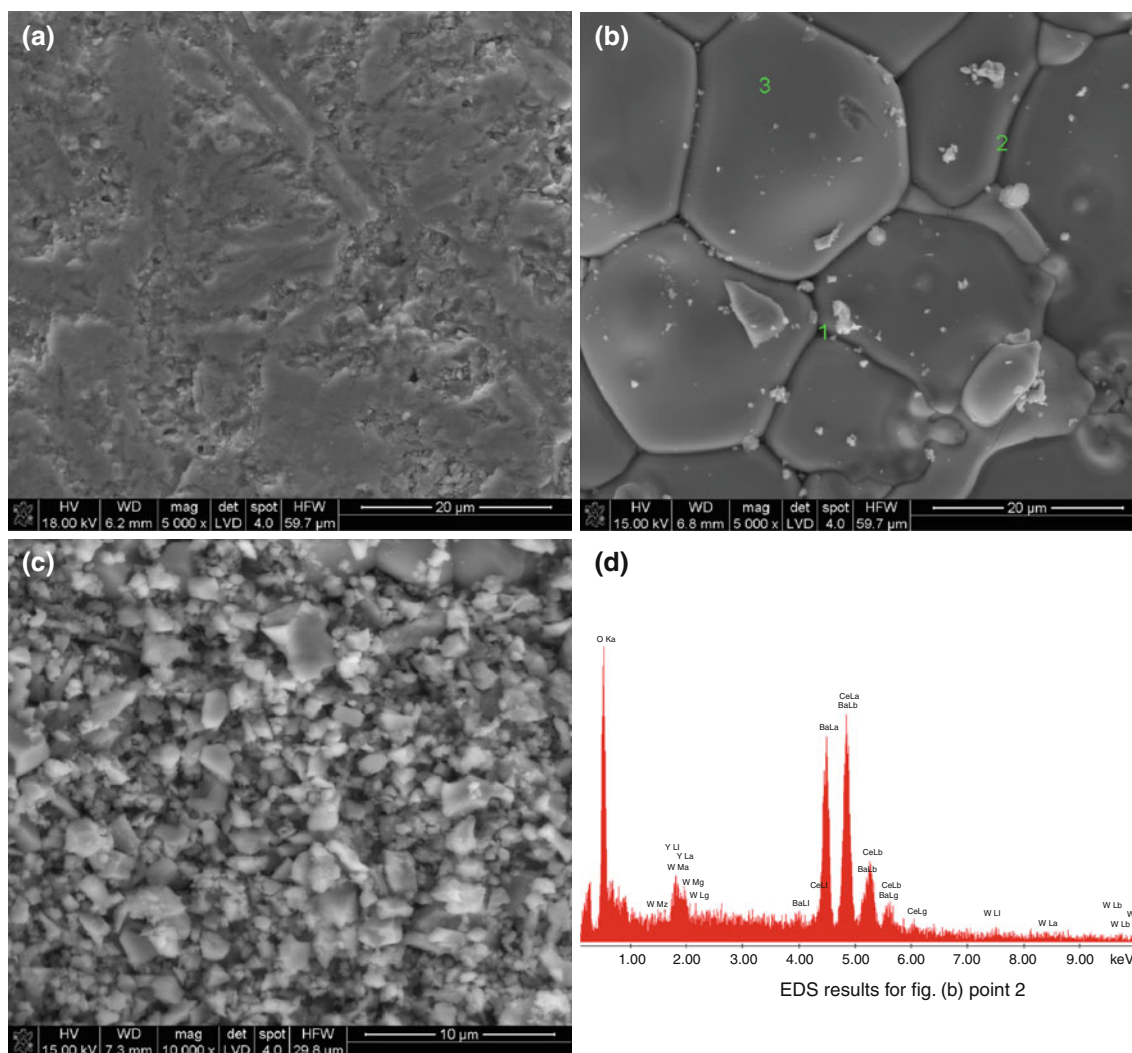


Fig. 3 Comparison of SEM microphotographs ($\times 5,000$) of samples with nominal composition: $\text{BaCe}_{0.9}\text{Y}_{0.1}\text{O}_3$ (a) and $0.9\text{BaCe}_{0.9}\text{Y}_{0.1}\text{O}_3-0.1\text{BaWO}_4$ (b), shown with SEM microphotograph ($\times 10,000$) of $\text{BaCe}_{0.9}\text{Y}_{0.1}\text{O}_3$ (c) and EDS results of $0.9\text{BaCe}_{0.9}\text{Y}_{0.1}\text{O}_3-0.1\text{BaWO}_4$ sample (d)

materials is significant. The disparity can be the result of different mechanisms of samples sintering. The sintering conditions were the same for both types of samples, so the differences observed in SEM images can be explained based on various compositions of these samples. Taking into account that barium tungstate melts at the temperature of about 1,475 °C [31], the sintering with the presence of liquid phase can be postulated in case of composite sample. In order to determine the distribution of tungsten phase, the EDS analysis of the grains and of the grain boundaries was performed (Fig. 3b). Figure 3d shows the example results of grain boundaries chemical analysis. Furthermore, the quantitative analysis indicates no significant difference between chemistry of grains and grain boundaries.

Based on the presented SEM images and the results of EDS analysis on the fractured surfaces, the presence of two phases can be verified. Unfortunately, the partition degree of tungsten between $\text{BaCe}(\text{Y,W})\text{O}_3$ and BaWO_4 phases cannot be quantified at this stage of research.

Summarizing the above, the XRD, SEM and EDS results indicate that tungsten both modifies the BaCeO_3 crystallographic structure and is present as the main constituent of the minor phase BaWO_4 . Both types of modifications caused by W introduction to the material may influence the most interesting properties of the material: chemical stability and electrical properties in a different ways.

Chemical stability

The main purpose of this study was to evaluate the possibility to improve the chemical stability of yttrium doped barium cerate by introduction of the second phase and formation of composite material. Literature survey clearly indicates that BaCeO_3 is unstable in some conditions, especially in the presence of CO_2 and H_2O [17, 18].

The determination of chemical stability was done using DTA-TG method supported by Evolved Gas Analysis (EGA) (Mass Spectrometry). These methods were found to be useful for such purposes [22]. All samples of single phase and composite materials were exposed to the atmosphere containing CO_2 and H_2O (7 % of CO_2 in air, 100 % RH) at 25 °C for 300 h. During such an exposition test, the reaction (3) takes place leading to the formation of secondary barium carbonate (and/or possibly hydroxide as an intermediate product). The amount of formed barium carbonate is proportional to the mass loss of sample during DTA-TG measurement and can be treated directly as a measure of chemical instability of material. Samples before and after exposition at the same conditions were compared. Figure 4 shows the TG data before the exposition to $\text{CO}_2/\text{H}_2\text{O}$ atmosphere of the samples: BaCeO_3 (reference sample), $\text{BaCe}_{0.9}\text{Y}_{0.1}\text{O}_3$ and $0.9\text{BaCe}_{0.9}\text{Y}_{0.1}\text{O}_3-0.1\text{BaWO}_4$.

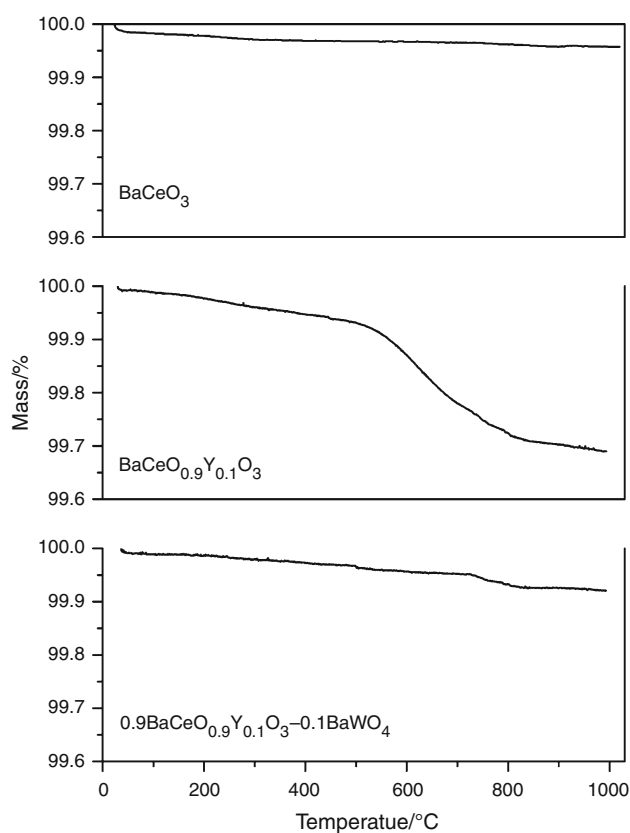


Fig. 4 TG curves of sinter samples BaCeO_3 , $\text{BaCe}_{0.9}\text{Y}_{0.1}\text{O}_3$ and $0.9\text{BaCe}_{0.9}\text{Y}_{0.1}\text{O}_3-0.1\text{BaWO}_4$ (nominal composition) before exposition test (7 % of CO_2 in air, 100 % RH, 300 h, 25 °C)

The TG data for the same samples, but after the exposition test, are presented in Fig. 5. The samples before the test exhibit only the slight mass loss: about 0.3 % in the case of yttrium-doped single phase material and less than 0.1 % for the rest of the samples. After the exposition test, relatively high and comparable mass losses (about 1.2 %) were observed for undoped and yttrium-doped barium cerates. According to the EGA results shown in Fig. 6, the water vapour and carbon dioxide were evolved gradually with temperature during the DTA-TG measurement, confirming that reaction (3) took place during the exposition test, and the adsorbed water and protonic defects were also present in the material. As reported previously [22], the total mass loss can be caused by liberation of both water vapour and CO_2 (as in the case of undoped BaCeO_3) or predominantly by carbon dioxide (as in the case of yttrium doped BaCeO_3). In the case of $0.9\text{BaCe}_{0.9}\text{Y}_{0.1}\text{O}_3-0.1\text{BaWO}_4$ composite material, much smaller mass loss (about 0.3 %) was determined, indicating the improvement of chemical stability compared to single phase materials.

The mechanism of improvement of chemical stability of $\text{BaCe}(\text{Y})\text{O}_3$ material due to introduction of tungsten may be discussed in terms of the modification of crystallographic structure (doping with W, most probably in Ce

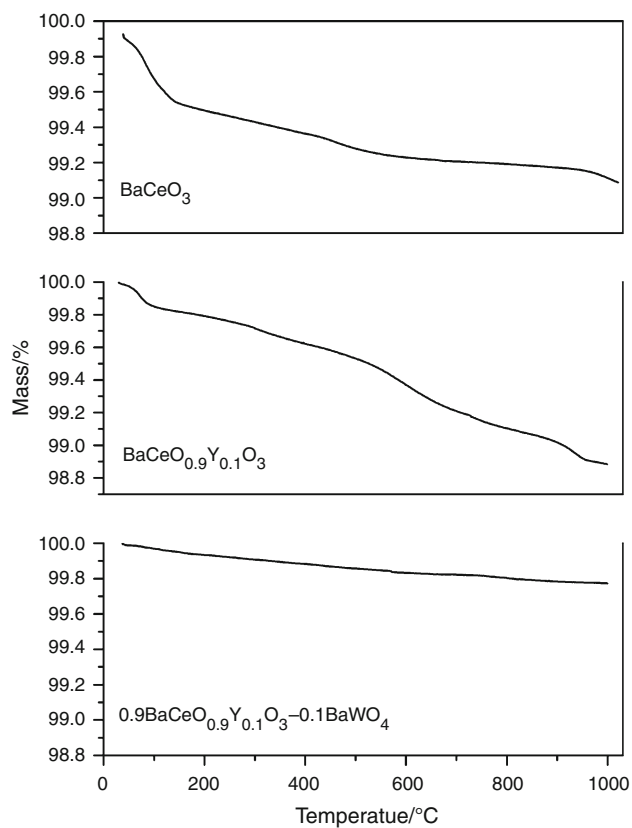


Fig. 5 TG curves of sinter samples BaCeO_3 , $\text{BaCe}_{0.9}\text{Y}_{0.1}\text{O}_3$ and $0.9\text{BaCe}_{0.9}\text{Y}_{0.1}\text{O}_3-0.1\text{BaWO}_4$ (nominal composition) after exposition test (7 % of CO_2 in air, 100 % RH, 300 h, 25 °C)

position) either by the formation of the second phase. Introduction of smaller W ion into the Ce ion position leads to the decrease of lattice parameters, as confirmed in this paper by XRD method and discussed above. In order to decide the mechanism of chemical stability improvement, the analysis based on Goldschmidt tolerance factor may be proposed. As reported previously in [8, 22, 32], the chemical stability of perovskite BaCeO_3 compounds is strongly correlated with the Goldschmidt tolerance factor, t . This parameter describes the deviation from ideal cubic perovskite structure, and can be calculated using the formula:

$$t = \frac{r_A + r_O}{\sqrt{2} \cdot (r_B + r_O)} \quad (6)$$

where, r_A is the ionic radius for A cation (Ba) for coordination number $\text{CN} = 12$, r_B the ionic radius for B cation (Ce) for coordination number $\text{CN} = 6$, r_O is the ionic radius for oxygen anions for coordination number $\text{CN} = 6$

For an ideal cubic structure, the Goldschmidt tolerance factor is equal to 1; for t values different from 1, the lower symmetric structures are observed. Moreover, the higher tolerance factor t , the better chemical stability can be postulated.

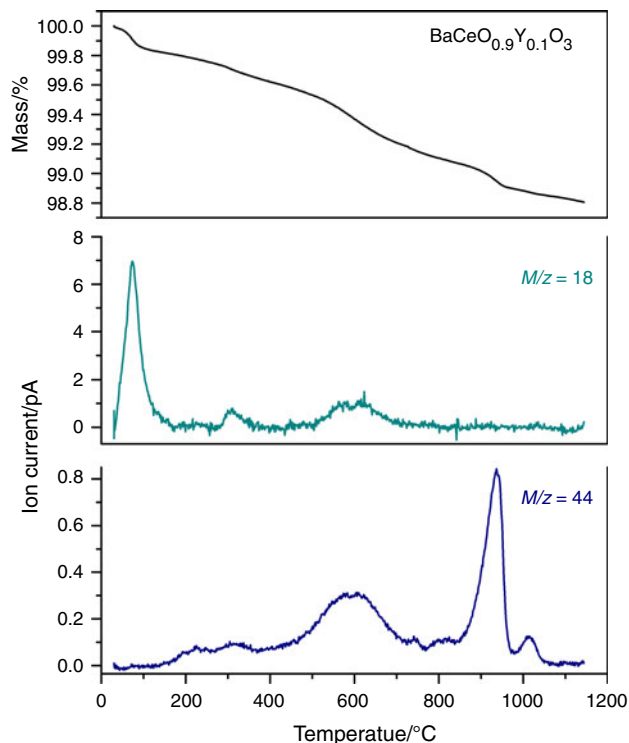


Fig. 6 TG/MS results of sinter sample $\text{BaCe}_{0.9}\text{Y}_{0.1}\text{O}_3$ (nominal composition) after exposition test (7 % of CO_2 in air, 100 % RH, 300 h, 25 °C)

In this paper, the theoretical values of S were calculated for $\text{BaCe}_{(1-x-y)}\text{Y}_x\text{W}_y\text{O}_3$ compound assuming that the $(r_B + r_O)$ distance is the linear combination of ionic radii of B cations (Ce, Y and W ions) according to the formula:

$$r_B + r_O = (1 - x - y)r_{\text{Ce}} + xr_{\text{Y}} + yr_{\text{W}} + r_O \quad (7)$$

where x and y describe the mole fraction of Y and W, respectively.

The $r_{\text{Ba}} = 0.161$ nm, $r_{\text{Ce}} = 0.087$ nm, $r_{\text{Y}} = 0.09$ nm, $r_{\text{W}} = 0.06$ nm, $r_{\text{O}} = 0.14$ nm values were used for calculation [33].

The introduction of W in the Ce position leads to the increase of Goldschmidt tolerance factor, calculated according to the formulas 6 and 7, as presented in Fig. 7. Moreover, doping of tungsten in Ce position leads to the decrease of lattice parameters and to the improvement of chemical stability. In consequence, the correlation between structure change described in terms of Goldschmidt tolerance factor and the improvement of chemical stability discussed above, can be easily found. It is in agreement with the results of [8, 32].

On the other hand, the improvement of chemical stability may be also explained by the introduction of the second phase and formation of composite material, as reported in [34] for $\text{Ce}_{0.8}\text{Sm}_{0.2}\text{O}_3-\text{BaCe}_{0.8}\text{Sm}_{0.2}\text{O}_3$ system. In such case, the second phase modifies mostly the grain

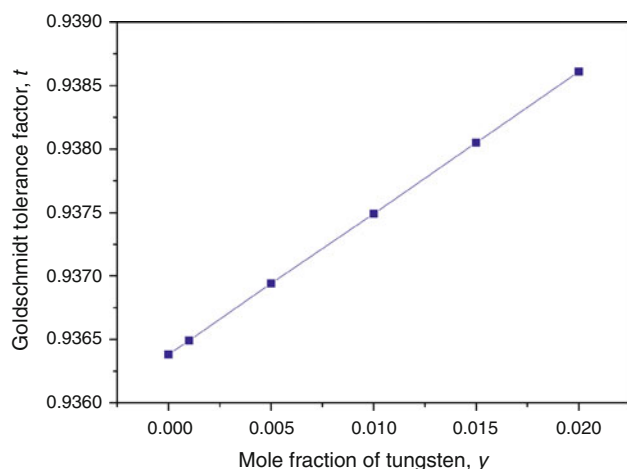


Fig. 7 Goldschmidt tolerance factor (t) as a function of mole fraction of tungsten (y) calculated for $\text{BaCe}_{(1-x-y)}\text{Y}_x\text{W}_y\text{O}_3$ compound

boundary properties, probably blocking the kinetics of any possible secondary reaction, thus leading to the improvement of chemical stability.

Based on presented results, it can be stated that both processes: incorporation of W into the Ce position and formation of the second phase of BaWO_4 are valid for our materials and can be the reason for chemical stability improvement.

Conclusions

In this study, the possibility of formation of composite material with $0.9\text{BaCe}_{0.9}\text{Y}_{0.1}\text{O}_{3-0.1}\text{BaWO}_4$ nominal composition was investigated. The development of such new materials based on BaCeO_3 protonic conductors was focused on the improvement of chemical stability. The synthesis of $\text{BaCe}_{1-x}\text{Y}_x\text{O}_{3-\delta}$ - BaWO_4 composite was found to be a difficult task due to some solubility of tungsten in BaCeO_3 lattice. The introduction of tungsten led to the modification of phase composition, crystallographic structure and microstructure of material. Namely, the decrease of lattice parameters was observed, most probably due to partial incorporation of W into the Ce position. In addition, the formation of BaWO_4 phase was identified, as expected. Moreover, the change of sintering mechanism involving the presence of liquid phase was observed, leading to the significant microstructure modification.

The determination of tungsten influence on chemical stability of BaCeO_3 materials was the main task of this study. Based on the DTA-TG results, it was found that the $0.9\text{BaCe}_{0.9}\text{Y}_{0.1}\text{O}_{3-0.1}\text{BaWO}_4$ composite material exhibits much better chemical stability towards the presence of CO_2 compared to the reference BaCeO_3 -based materials. The discussion of the chemical stability improvement mechanism

was also presented. Two found processes caused by tungsten: structure modification and development of composite two phase material can be considered as possible methods to secure the satisfactory chemical stability for potential applications of proposed new material.

Acknowledgments The financial support of Polish National Science Centre (NCN), Project No. DEC 2011/01/B/ST5/06427 (AGH No. 18.18.160.189) is acknowledged.

Open Access This article is distributed under the terms of the Creative Commons Attribution License which permits any use, distribution, and reproduction in any medium, provided the original author(s) and the source are credited.

References

- Matsumoto H, Asakura F, Takeuchi K, Iwahara H. Transient phenomena of an electrochemical hydrogen pump using a SrCeO_3 -based proton conductor. *Solid State Ionics*. 2000;129:209–18.
- Fabrizi E, D'Epifanio A, Di Bartolomeo E, Licocchia S, Traversa E. Tailoring the chemical stability of $\text{Ba}(\text{Ce}_{0.8-x}\text{Zr}_x)\text{Y}_{0.2}\text{O}_{3-\delta}$ protonic conductors for Intermediate Temperature Solid Oxide Fuel Cells (IT-SOFCs). *Solid State Ionics*. 2008;179:558–64.
- Kreuer KD. On the development of proton conducting materials for technological applications. *Solid State Ionics*. 1997;97:1–15.
- Zhao F, Wang S, Dixon L, Chen F. Novel $\text{BaCe}_{0.7}\text{In}_{0.2}\text{Yb}_{0.1}\text{O}_{3-\delta}$ proton conductor as electrolyte for intermediate temperature solid oxide fuel cells. *J Power Sources*. 2011;196:7500–4.
- Bezerra Lopes FW, Arab M, de Pereira Souza HPMC, de Fernandes Souza J, Gavarri JR. High temperature conduction and methane conversion capability of BaCeO_3 perovskite. *Powder Technol*. 2012;219:186–92.
- Iwahara H, Esaka T, Uchida H, Maeda N. Proton conduction in sintered oxides and its application to steam electrolysis for hydrogen production. *Solid State Ionics*. 1981;3–4:359–63.
- Iwahara H, Uchida H, Ono K, Ogaki K. Proton conduction in sintered oxides based on BaCeO_3 . *J Electrochem Soc*. 1988;135:529–33.
- Haile SM, Stanoff G, Ryu KH. Non-stoichiometry, grain boundary transport and chemical stability of proton conducting perovskites. *J Mater Sci*. 2001;36:1149–60.
- Vaquero-Aguilar C, Jiménez-Melendo M. Characterization and creep properties of proton-conducting Yb-doped barium cerate. *J Eur Ceram Soc*. 2011;31:2671–6.
- Radojković A, Žunić M, Savić SM, Branković G, Branković Z. Enhanced stability in CO_2 of Ta doped $\text{BaCe}_{0.9}\text{Y}_{0.1}\text{O}_{3-\delta}$ electrolyte for intermediate temperature SOFCs. *Ceram Int*. 2013;39:2631–7.
- Sawant P, Varma S, Wani BN, Bharadwaj SR. Influence of synthesis route on morphology and conduction behavior of $\text{BaCe}_{0.8}\text{Y}_{0.2}\text{O}_3$. *J Therm Anal Calorim*. 2012;107:189–95.
- Oishi M, Akoshima S, Yashiro K, Sato K, Mizusaki J, Kawada T. Defect structure analysis of B-site doped perovskite-type proton conducting oxide BaCeO_3 Part 1: the defect concentration of $\text{BaCe}_{0.8}\text{M}_{0.1}\text{O}_{3-\delta}$ ($\text{M} = \text{Y}$ and Yb). *Solid State Ionics*. 2009;180:127–31.
- Oishi M, Akoshima S, Yashiro K, Sato K, Mizusaki J, Kawada T. Defect structure analysis of B-site doped perovskite-type proton conducting oxide BaCeO_3 : part 2: the electrical conductivity and diffusion coefficient of $\text{BaCe}_{0.9}\text{M}_{0.1}\text{O}_{3-\delta}$. *Solid State Ionics*. 2008;179:2240–7.

14. Oishi M, Akoshima S, Yashiro K, Sato K, Kawada T, Mizusaki J. Defect structure analysis of proton-oxide ion mixed conductor $\text{BaCe}_{0.9}\text{Nd}_{0.1}\text{O}_{3-\delta}$. *Solid State Ionics*. 2010;181:1336–43.
15. Chen FL, Sørensen OT, Meng GY, Peng DK. Preparation of Nd-doped BaCeO_3 proton-conducting ceramic and its electrical properties in different atmospheres. *J Eur Ceram Soc*. 1998;18:1389–95.
16. Takeuchi K, Loong CK, Richardson JW Jr, Guan J, Dorris SE, Balachandran U. The crystal structures and phase transitions in Y-doped BaCeO_3 : their dependence on Y concentration and hydrogen doping. *Solid State Ionics*. 2000;138:63–77.
17. Ryu KH, Haile SM. Chemical stability and proton conductivity of doped BaCeO_3 – BaZrO_3 solid solutions. *Solid State Ionics*. 1999;125:355–67.
18. Ma G, Shimura T, Iwahara H. Ionic conduction and nonstoichiometry in $\text{Ba}_x\text{Ce}_{0.90}\text{Y}_{0.10}\text{O}_{3-\delta}$. *Solid State Ionics*. 1998;110:103–10.
19. Kreuer KD. Proton-conducting oxides. *Annu Rev Mater Res*. 2003;33:333–59.
20. Medvedev DA, Gorbova EV, Demin AK, Antonov BD. Structure and electric properties of $\text{BaCe}_{0.77-x}\text{Zr}_x\text{Gd}_{0.2}\text{Cu}_{0.03}\text{O}_{3-\delta}$. *Russ J Electrochem*. 2011;47:1404–10.
21. Katahira K, Kohchi Y, Shimura T, Iwahara H. Protonic conduction in Zr-substituted BaCeO_3 . *Solid State Ionics*. 2000;138:91–8.
22. Pasierb P, Drożdż-Cieśla E, Gajerski R, Łabuś S, Komornicki S, Rękas M. Chemical stability of $\text{Ba}(\text{Ce}_{1-x}\text{Ti}_x)_{1-y}\text{Y}_y\text{O}_3$ proton-conducting solid electrolytes. *J Therm Anal Calorim*. 2009;96:475–80.
23. Talimi M, Thangadurai V. Electrical conductivity and chemical stability of perovskite-type $\text{BaCe}_{0.8-x}\text{Ti}_x\text{Y}_{0.2}\text{O}_{3-\delta}$. *Ionics*. 2011;17:195–200.
24. Tamaki J, Fujii T, Fujimori K, Miura N, Yamazoe N. Application of metal tungstate-carbonate composite to nitrogen oxides sensor operative at elevated temperature. *Sens Actuat B-Chem*. 1995;24–25:396–9.
25. Shan Z, Wang Y, Ding H, Huang F. Structure-dependent photocatalytic activities of MWO_4 ($\text{M} = \text{Ca}, \text{Sr}, \text{Ba}$). *J Mol Catal A-Chem*. 2009;302:54–8.
26. Zhuang H, Yue Z, Zhao F, Pei J, Li L. Microstructure and microwave dielectric properties of $\text{Ba}_5\text{Nb}_4\text{O}_{15}$ – BaWO_4 composite ceramics. *J Alloy Compd*. 2009;472:411–5.
27. Al-Hajji LA, Hasan MA, Zaki MI. Kinetics of formation of barium tungstate in equimolar powder mixture of BaCO_3 and WO_3 . *J Therm Anal Calorim*. 2010;100:43–9.
28. Kim YK, Lee KM, Jang HM. 1:2 Long-range ordering and defect mechanism of WO_3 -doped perovskite $\text{Ba}(\text{Mg}_{1/3}\text{Ta}_{2/3})\text{O}_3$. *J Mater Sci*. 2000;35:4885–93.
29. Melnikov P, Nascimento VA, Consolo LZZ, Silva FA. Mechanism of thermal decomposition of yttrium nitrate hexahydrate, $\text{Y}(\text{NO}_3)_3 \cdot 6\text{H}_2\text{O}$ and modeling of intermediate oxynitrates. *J Therm Anal Calorim*. 2013;111:115–9.
30. Madarász J, Szilágyi IM, Hange F, Pokol G. Comparative evolved gas analyses (TG-FTIR, TG/DTA-MS) and solid state (FTIR, XRD) studies on thermal decomposition of ammonium paratungstate tetrahydrate (APT) in air. *J Anal Appl Pyrolysis*. 2004;72:197–201.
31. Voronina IS, Ivleva LI, Basiev TT, Zverev PG, Polozkov NM. Active Raman media: $\text{SrWO}_4:\text{Nd}^{3+}$, $\text{BaWO}_4:\text{Nd}^{3+}$. Growth and characterization. *J Optoelectron Adv M*. 2003;5:887–92.
32. Takayama-Muromachi E, Navrotsky A. Energetics of compounds ($\text{A}^{2+}\text{B}^{4+}\text{O}_3$) with the perovskite structure. *J Solid State Chem*. 1988;72:244–56.
33. Shannon RD. Revised effective ionic radii and systematic studies of interatomic distances in halides and chalcogenides. *Acta Crystallogr*. 1976;A32:751–67.
34. Medvedev D, Maragou V, Pikalova E, Demin A, Tsiakaras P. Novel composite solid state electrolytes on the base of BaCeO_3 and CeO_2 for intermediate temperature electrochemical devices. *J Power Sources*. 2013;221:217–27.